NASA TECHNICAL MEMORANDUM

NASA TM X-1777

NASA TM X-1777

EXPERIMENTAL INVESTIGATION OF A 10° CONICAL TURBOJET PLUG NOZZLE WITH TRANSLATING PRIMARY AND SECONDARY SHROUDS AT MACH NUMBERS FROM 0 TO 2.0

by Donald L. Bresnahan

Lewis Research Center
Cleveland, Ohio

NATIONAL AERONAUTICS AND SPACE ADMINISTRATION • WASHINGTON, D. C. • APRIL 1969

NASA TM X-1777

EXPERIMENTAL INVESTIGATION OF A 10° CONICAL TURBOJET PLUG NOZZLE WITH TRANSLATING PRIMARY AND SECONDARY SHROUDS AT MACH NUMBERS FROM 0 TO 2.0

By Donald L. Bresnahan

Lewis Research Center
Cleveland, Ohio

NATIONAL AERONAUTICS AND SPACE ADMINISTRATION

For sale by the Clearinghouse for Federal Scientific and Technical Information
Springfield, Virginia 22151 – CFSTI price $3.00

ABSTRACT

Nozzle efficiencies and pumping characteristics were measured with and without external flow for a configuration employing a translating primary shroud for throat area variation. Efficiencies are compared with those of an alternate configuration employing an iris-type primary shroud. Both configurations were appropriate for an afterburning turbojet engine cycle. At subsonic speeds with the cylindrical secondary shroud retracted, the nozzles performed about the same. However, with the secondary shroud extended for operation at supersonic speeds, the translating primary provided a lower efficiency at the full-afterburning position. The pumping characteristics of the translating primary shroud were such that secondary flow could be provided to cool the primary nozzle and the shroud at all flight conditions except takeoff.

EXPERIMENTAL INVESTIGATION OF A 10° CONICAL TURBOJET PLUG NOZZLE WITH TRANSLATING PRIMARY AND SECONDARY SHROUDS AT MACH NUMBERS FROM 0 TO 2.0

by Donald L. Bresnahan

Lewis Research Center

SUMMARY

An experimental investigation was conducted in a nozzle static test facility and the 8- by 6-Foot Supersonic Wind Tunnel to determine the performance characteristics of a 10° half-angle conical turbojet plug nozzle with a translated primary shroud for throat area modulation. The internal expansion of the nozzle was adjusted by translating a cylindrical secondary shroud. The results were then compared with the efficiency of an iris-type primary with the same throat area, tested under identical conditions.

Subsonically, with the secondary shroud retracted, the nozzles performed about the same. Supersonically, however, with the secondary shroud extended, the efficiency of the translating primary at the full-afterburning position fell below that of the iris primary. The trend indicated a further deterioration in nozzle efficiency at higher Mach numbers and pressure ratios.

The pumping characteristics of the nozzle were such that secondary flow could be provided to cool the primary nozzle and the shroud at all flight conditions except take-off. In general, optimum efficiency was obtained near the geometric choking corrected secondary weight flow ratio.

INTRODUCTION

In the continuing study of airbreathing propulsion at the Lewis Research Center, plug nozzles are receiving considerable emphasis. They offer the potential of good aerodynamic performance together with reduced mechanical complexity and a consequent reduction in maintenance. References 1 and 2 document the aerodynamic performance of

plug nozzle configurations with simulated translating secondary shrouds suitable for nonafterburning and afterburning turbojet engines, respectively, designed for cruise at a Mach number near 2.7. A high level of nozzle efficiency was maintained over a wide range of pressure ratios by extending the cylindrical secondary shroud to increase the internal expansion as nozzle pressure ratio increased.

To provide for changes in engine-operating conditions, such as afterburning, the nozzle must have a variable throat. This area variation can be accomplished in several ways with a plug nozzle. It can have an iris primary (ref. 2), a variable-diameter plug (ref. 3), or relative translation between the primary shroud and the plug. The third method could be mechanically simpler in that it may not have as complex a sealing problem as the other two methods.

As a continuation of the work in reference 2, an investigation was conducted to determine the afterburner-on performance of a plug nozzle with a fixed centerbody and simulated translated primary shroud for throat area modulation. The translated primary shroud throat area was the same as the iris primary throat area (20.45 sq in., 131.90 sq cm) of reference 2, a 40-percent increase over the afterburner-off configuration. A 10° half-angle plug nozzle with a simulated translating cylindrical secondary shroud and an overall afterburner-off design pressure ratio of 26.3 was tested in a nozzle static test facility to investigate quiescent performance and in the 8- by 6-Foot Supersonic Wind Tunnel at Mach numbers up to 1.97 to determine external flow effects. Shroud cooling flow was studied at corrected secondary weight flow ratios to 8 percent of the primary weight flow to determine the effect on performance. Dry air at room temperature was used for primary and secondary flows in both facilities. Maximum nozzle pressure ratios of 18 were obtained.

SYMBOLS

A	area
D	drag
d	model diameter
F	thrust
l	full plug length measured from nozzle throat with afterburner off
M	Mach number
P	total pressure
p	static pressure

r radius

T total temperature

w weight-flow rate

x axial distance measured from nozzle throat with afterburner off

y radial distance in plane of primary total-pressure rake

θ circumferential position

Subscripts:

bt boattail

i ideal

j jet

max maximum

p primary

s secondary

x condition at distance x

0 free stream

7 nozzle inlet

8 nozzle throat

9 nozzle exit

APPARATUS AND INSTRUMENTATION

Installation in Static Test Facility

The research hardware installation in the static test facility is shown in figures 1 and 2. The nozzles were mounted on a section of pipe attached to the bedplate, which was freely suspended by four flexure rods. Pressure forces acting on the nozzle and mounting pipe, both external and internal, were transmitted from the bedplate through a bell crank to a calibrated balanced-air-pressure diaphragm which measured thrust. Two labyrinth seals around the necked-down inlet section ahead of the mounting pipe separated the nozzle-inlet air from the exhaust. The space between the two labyrinth seals was vented to the test chamber. This decreased the pressure differential across

the second labyrinth and prevented a pressure gradient on the outside of the diffuser section caused by an air blast from under the labyrinth seal.

Pressures and temperatures were measured at the various stations indicated. Total and wall static-pressure measurements were used at the bellmouth inlet to compute inlet momentum, and at the primary air-metering station to compute the primary airflow. The nozzle inlet total pressure and temperature were measured at station 7, and ambient exhaust pressure at station 0.

Installation in 8- by 6-Foot Supersonic Wind Tunnel

The 8- by 6-Foot Supersonic Wind Tunnel model support system and its internal geometry and thrust-measuring system are shown schematically in figure 3. The grounded portion of the model was supported from the tunnel ceiling by a thin vertical strut with a 50.25-inch (127.63-cm) chord and a thickness-to-chord ratio of 0.035. The floating portion, which is composed of the primary and secondary air bottles and the exhaust nozzle, is cantilevered by flow tubes from external supply manifolds. The primary air bottle was supported by front and rear bearings. The secondary air passed through hollow struts at station 100.66 (255.68 cm) to the annulus formed between the primary and secondary shrouds. The axial force of the nozzle, which included secondary flow effects, was transmitted to the load cell located in the nose of the model. Since the floating portion of the model included a portion of the afterbody and boattail, the measured force included some external skin friction drag and the boattail drag.

A static calibration of the thrust-measuring system was obtained by applying known forces to the nozzle and measuring the output of the load cell. A water-cooled jacket surrounded the load cell and maintained a constant temperature of 90° F (305.5 K) to eliminate errors in the calibration caused by variations in temperature from aerodynamic heating.

Nozzle Configurations

The nozzle configurations consisted of a 10° half-angle plug with three secondary shrouds of different lengths to simulate translation. Basic nozzle dimensions are shown in figure 4. The afterburning nozzle simulated a translation of the afterburner-off primary shroud reported in reference 2 to a position providing a 40-percent increase in throat area for afterburner-on operation, as indicated in figure 4. The projected area of the primary shroud was about 20 percent of the maximum model area. The overall design pressure ratio was 26.3 for the afterburner-off operation. The maximum

model diameter was 8.5 inches (21.59 cm) with a circular arc boattail on the shroud to minimize drag. The projected area of the boattail was about 11.5 percent of the maximum model area. In figures 4(b) and 5 are shown the shroud extensions that were tested. Variations in nozzle area ratio and internal expansion pressure ratio with shroud position are shown in figure 6 for an afterburner-off configuration and afterburner-on configurations with iris and translating primary shrouds. The curves indicate the area ratio variation for a translating secondary shroud. Tick marks on the curves indicate the shroud positions that were tested. The primary throat was the reference point for the shroud length to diameter ratio, x/d. With secondary shroud retracted to negative x/d positions, the nozzle has a sonic discharge, and the internal area ratio is defined as 1. As the shroud is extended past the primary lip, the final internal area A_9 transfers from the primary area to the annular internal flow area between the plug and secondary shroud causing an abrupt increase in area ratio. The curves extend to the length to diameter ratio corresponding to the plug tip location.

The model instrumentation is shown in figure 7. The primary and secondary total pressures were obtained by use of total-pressure probes (fig. 7(a)). The primary rake was area weighted. Typical primary-rake pressure profiles are shown in figure 7(b). The primary shroud boattail instrumentation is shown in figure 7(c). A row of static-pressure orifices was located on the plug at a meridian angle of 180° (fig. 7(d)).

PROCEDURE

Static Test Facility

Pressure ratios were set by maintaining a constant nozzle inlet pressure and varying the exhaust pressure. Each configuration was tested over a range of pressure ratios which were appropriate for the particular shroud extension ratio.

8- by 6-Foot Supersonic Wind Tunnel

Nozzle performance was obtained over a range of pressure ratios at several Mach numbers for each shroud length tested. Since tunnel static pressure was fixed at a given Mach number, the nozzle pressure ratio was varied by changing the nozzle inlet pressure. The maximum pressure ratio at each Mach number was restricted because of the limitations of the primary air supply. The highest pressure ratio obtained was approximately 18 at Mach 1.97.

DATA REDUCTION

Static Test Facility

The nozzle primary airflow was calculated from pressure and temperature measurements at the air-metering station (fig. 1) and an effective area determined by an ASME calibration nozzle. The secondary airflow was measured by means of a standard ASME flowmetering orifice in the external supply line.

Actual jet thrust was calculated from thrust-cell measurements corrected for tare forces. The ideal jet thrust for each of the primary and secondary flows was calculated from the measured mass flow rate expanded from their measured total pressures to p_0. Provision was made to equate the ideal thrust of the secondary flow to zero if the total pressure was less than p_0. Data where this condition existed are identified on the curves. Nozzle efficiency is defined then as the ratio of the actual jet thrust to the ideal thrust of both primary and secondary flows:

$$\text{Nozzle static efficiency} = \frac{F_j}{F_{ip} + F_{is}}$$

In addition, the nozzle gross thrust coefficient F_j/F_{ip} is also presented.

8- by 6-Foot Supersonic Wind Tunnel

Both primary and secondary flow rates were measured by means of standard ASME flowmetering orifices located in the external supply lines. Thrust-minus-drag measurements were obtained from a load cell readout of the axial forces acting on the floating portion of the model. Internal tare forces, determined by internal areas and measured tare pressures located as shown in figure 3, were accounted for in the thrust calculation.

The only external friction drag charged to the nozzle is that downstream of station 113.49 (288.3 cm), shown in figure 3. That force acting on the portion of the nozzle between stations 93.65 (237.9 cm) and 113.49 (288.3 cm) was also measured on the load cell, but is not considered to be part of the nozzle drag. Its magnitude was estimated by using the semiempirical flat-plate mean skin friction coefficient given in figure 7 of reference 4 as a function of free-stream Mach number and Reynolds number. The coefficient accounts for variations in boundary-layer thickness and profile with Reynolds number. Previous measurements of the boundary-layer characteristics at the aft end

of this jet exit model in the 8- by 6-Foot Supersonic Wind Tunnel indicated that the profile and thickness were essentially the same as that computed for a flat plate of equal length. The strut wake appeared to affect only a localized region near the top of the model and resulted in a slightly lower local free-stream velocity than measured on the side and bottom of the model. Therefore, the results of reference 4 were used without correction for three-dimensional flow effects or strut interference effects. The resulting correction was applied to the load cell force.

The ideal jet thrust for each of the primary and secondary flows was calculated from the measured mass flow rate expanded from their measured total pressures to p_0. Provision was made to equate the ideal thrust of the secondary flow to zero if the total pressure was less than p_0. Data where this condition exists are identified on the curves. Nozzle efficiency is defined then as the ratio of the thrust-minus-drag to the ideal thrust of both primary and secondary flows:

$$\text{Nozzle efficiency} = \frac{F - D}{F_{ip} + F_{is}}$$

In addition, the nozzle gross thrust coefficient $(F - D)/F_{ip}$ is also presented.

RESULTS AND DISCUSSION

A full-length plug nozzle was tested with three secondary shrouds of different lengths to simulate translation and a translated primary shroud to simulate an afterburner-on condition. The longest secondary shroud extension tested was the shortest determined to give near optimum performance at supersonic cruise in reference 2. Each configuration was tested over a range of nozzle pressure ratios and Mach numbers determined by the design pressure ratio for the shroud length and a typical schedule for a supersonic turbojet engine (fig. 8). The results are compared with the efficiency of an iris-type primary shroud reported in reference 2.

These configurations were tested over a range of pressure ratios and Mach numbers from takeoff to Mach 2.0. The gross thrust coefficient without secondary flow is shown in figure 9, and the nozzle efficiency with 4-percent corrected secondary flow ratio in figure 10. High efficiencies were obtained with the secondary shroud retracted at subsonic speeds and extended at supersonic speeds. The intermediate shroud length did not perform as well. In this position the secondary shroud lip is just downstream of the primary shroud lip and therefore is not controlling the flow expansion. The lower performance then is a result of the combined effects of excessive expansion and divergence losses and drag from the blunt base formed by the secondary shroud and primary

lip. A comparison of the three shroud lengths tested is made in figure 11 over a range of Mach numbers. This indicates that for the flight schedule selected and the translated primary shroud, a two-position secondary shroud which is either fully retracted or fully extended would give near optimum performance. The nozzle gross thrust coefficient for these configurations is shown in figure 12 for 4-percent corrected secondary flow ratio.

To minimize the drag induced by the internal base formed between the primary shroud and the extended secondary shroud, and for shroud-cooling purposes, some secondary flow is required. With the shroud retracted, secondary flow would be discharged through the annular gap at the shoulder of the primary shroud afterbody. The effect of secondary flow on nozzle efficiency is shown in figure 13, and the nozzle gross thrust coefficient is shown in figure 14 for the range of secondary flows studied. The effect of secondary flow on the primary shroud boattail pressures is shown in figure 15, and the corresponding secondary total-pressure ratio requirements (or pumping characteristics) are presented in figure 16. In general, the peaks of both the efficiency and the primary boattail pressure curves occurred at corrected secondary weight flow ratios of from 0.02 to 0.04.

As indicated in sketch a, secondary flow choking may occur at two locations. With the jet attached to the secondary shroud, an aerodynamic choke point for the secondary flow would exist near the attachment point. If the secondary flow rate is increased sufficiently, a second choke point can exist at the minimum geometric secondary flow area upstream of the boattail. Under these conditions the secondary flow can become supersonic at all stations downstream of the geometric choke point. If the aerodynamic choke point is eliminated either by operating the nozzle at such low primary pressure ratios that the jet is detached from the secondary shroud or by translating the secondary shroud upstream so that jet attachment cannot occur, then only geometric choking of the secondary flow can occur.

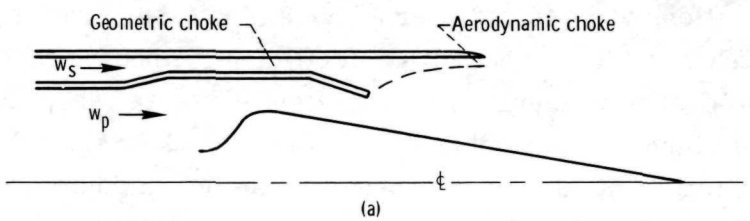

(a)

The secondary pressure ratio required to cause geometric choking is indicated in figure 16 for each of the secondary shroud positions. With the long secondary shroud extension (fig. 16(c)), the secondary total-pressure ratio was independent of primary nozzle pressure ratio over the range investigated indicating that the primary jet was attached to the secondary shroud and, hence, that aerodynamic choking of the secondary flow existed. At secondary weight flow ratios of about 0.04 and greater, the pumping curve became coincident with the geometric choke line. As indicated in figures 13(c) and 15(c), respectively, the nozzle efficiency and primary boattail pressures were greatest just as geometric choking began to occur $\left((w_s/w_p)\sqrt{T_s/T_p} = 0.04\right)$. At higher secondary flows, where the secondary flow became supersonic, the boattail pressures and nozzle efficiency decreased. With the retracted shroud positions (figs. 16(a) and (b)), only geometric choking was evident at secondary flow ratios of 0.04 or greater depending on nozzle pressure ratio. Figures 13(a) and (b) and also figures 15(a) and (b) again indicate that peak efficiency and peak boattail pressures tended to occur at the minimum secondary flow ratio which caused geometric choking.

The pressure recovery needed to supply the secondary flow is shown in figure 17. At takeoff, with the shroud retracted, there is no pumping; as a result, any secondary flow would have to come from the engine cycle. With external flow, at the subsonic and supersonic speeds shown, the pumping is such that corrected secondary flow ratios as large as approximately 7 percent could be obtained from inlets.

External flow effects on plug pressure distributions are shown in figure 18 for selected pressure ratios and Mach numbers for the shroud position giving the highest efficiency. There was good agreement between the two facilities at $M_0 = 0$ (fig. 18(a)). Differences in nozzle pressure ratio between the two facilities resulted in some pressure differences upstream of the nozzle throat in some of the figures. The external flow effects on pressures downstream of the throat were negligible at most Mach numbers with the greatest effect occurring at Mach 1.2 with the shroud retracted (fig. 18(d)). At this Mach number there was a greater overexpansion on the plug surface; however, it occurs downstream of the 50-percent point on the plug where the projected area is relatively small. For this condition, the plug force downstream of the nozzle throat accounted for 2.12 percent of the nozzle thrust statically, while at Mach 1.2 it accounted for 1.88 percent.

A comparison of the efficiency of the translated primary to the iris primary of reference 2 is made in figure 19. Each curve represents the optimum efficiency of the shrouds tested based on the operating schedule of figure 8. The selection of the secondary flow rate was based on anticipated cooling requirements.

Subsonically with the shroud retracted, the nozzles performed about the same. Supersonically, however, with the shroud extended, the efficiency of the translated primary fell below the iris primary with a trend indicating a further deterioration in

nozzle efficiency at higher Mach numbers and pressure ratios. This is due to the increased divergence losses and the larger primary boattail area of the translated primary. The translating primary shroud retains a fixed base area in the afterburning on and off positions. The outer base diameter is determined by flow area requirements at the maximum plug radius with the afterburner on, and the inner base diameter is dictated by throat area requirements during afterburner-off conditons. This large base is translated downstream during afterburner operation, providing a large expansion angle between the primary and secondary shroud lips resulting in excessive divergence losses. The iris primary provides the advantages of a low base area and a low expansion angle during afterburner operation, which produces improved performance. It is possible that a longer shroud extension may have increased the translated primary nozzle efficiency at the higher Mach numbers.

SUMMARY OF RESULTS

An earlier plug nozzle test investigated fixed primary shrouds simulating afterburner on and off operation with throat area variation provided by an iris primary nozzle. The present plug nozzle simulated afterburner operation with the area increase obtained by translation of the primary shroud investigated earlier for afterburner-off operation. Experimental data were analyzed and compared with similar data for the simulated iris primary with the following results:

1. High nozzle efficiencies were obtained subsonically with the shroud retracted and supersonically with the shroud extended. The intermediate shroud length had poor performance probably because of the combined effects of excessive expansion and divergence losses and drag from the blunt base formed by the secondary shroud and primary lip.

2. The pumping characteristics of the nozzle were such that secondary flow could be provided to cool the primary nozzle and the shroud at all flight conditions except takeoff.

3. In general, the base pressure and nozzle efficiency curves peaked near the geometric choking secondary weight flow ratio.

4. Subsonically with the secondary shroud retracted, the iris and translating primary shrouds performed about the same. Supersonically, however, with the secondary shroud extended, the efficiency of the translating primary fell below the iris primary. The trend indicated a further deterioration in nozzle efficiency at higher Mach numbers and pressure ratios. This loss of efficiency appeared to be due to the larger primary shroud base and the larger angle between the primary and secondary

shroud lips which permitted excessive divergence losses. It is possible that a longer shroud extension would better control the flow expansion and increase the nozzle efficiency.

Lewis Research Center,
National Aeronautics and Space Administration,
Cleveland, Ohio, November 26, 1968,
126-15-02-10-22.

REFERENCES

1. Bresnahan, Donald L.; and Johns, Albert L.: Cold Flow Investigation of a Low Angle Turbojet Plug Nozzle With Fixed Throat and Translating Shroud at Mach Numbers From 0 to 2.0. NASA TM X-1619, 1968.

2. Bresnahan, Donald L.: Experimental Investigation of a 10^{o} Conical Turbojet Plug Nozzle With Iris Primary and Translating Shroud at Mach Numbers From 0 to 2.0. NASA TM X-1709, 1968.

3. Wasko, Robert A.; and Harrington, Douglas E.: Performance of a Collapsible Plug Nozzle Having Either Two-Position Cylindrial or Variable Angle Floating Shroud at Mach Numbers From 0 to 2.0. NASA TM X-1657, 1968.

4. Smith, K. G.: Methods and Charts for Estimating Skin Friction Drag in Wind Tunnel Tests With Zero Heat Transfer. ARC CP-824, Aeronautical Research Council, Great Britain, 1965. (Available from DDC as AD-487132.)

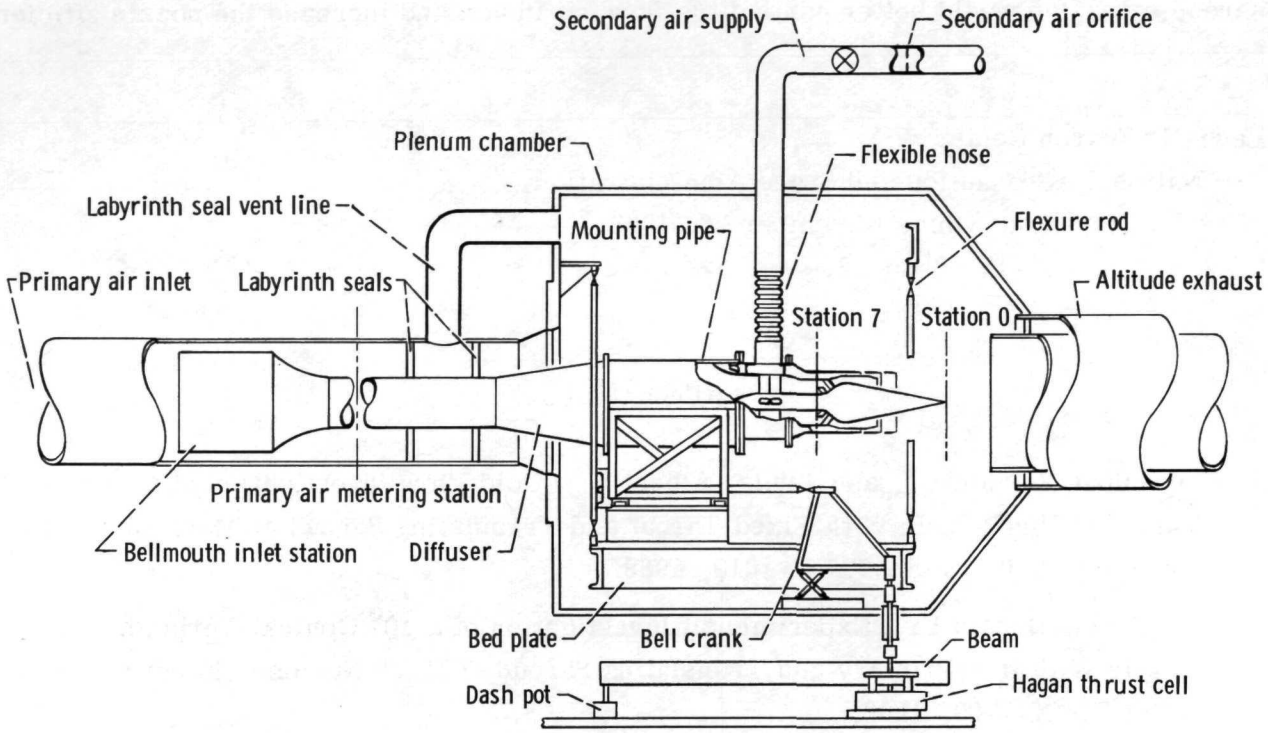

Figure 1. - Schematic view of static test stand.

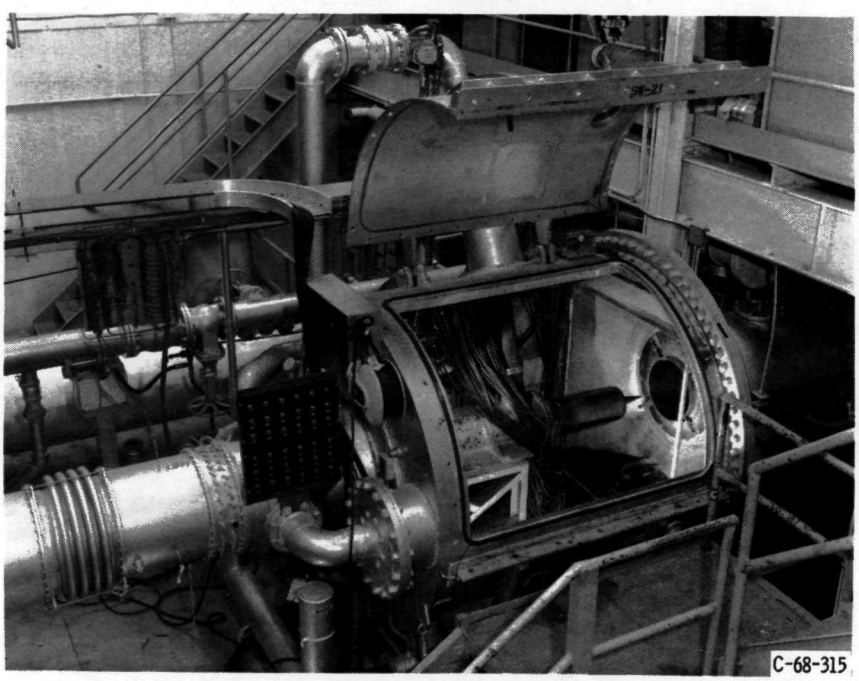

Figure 2. - Installation of nozzle in static test facility.

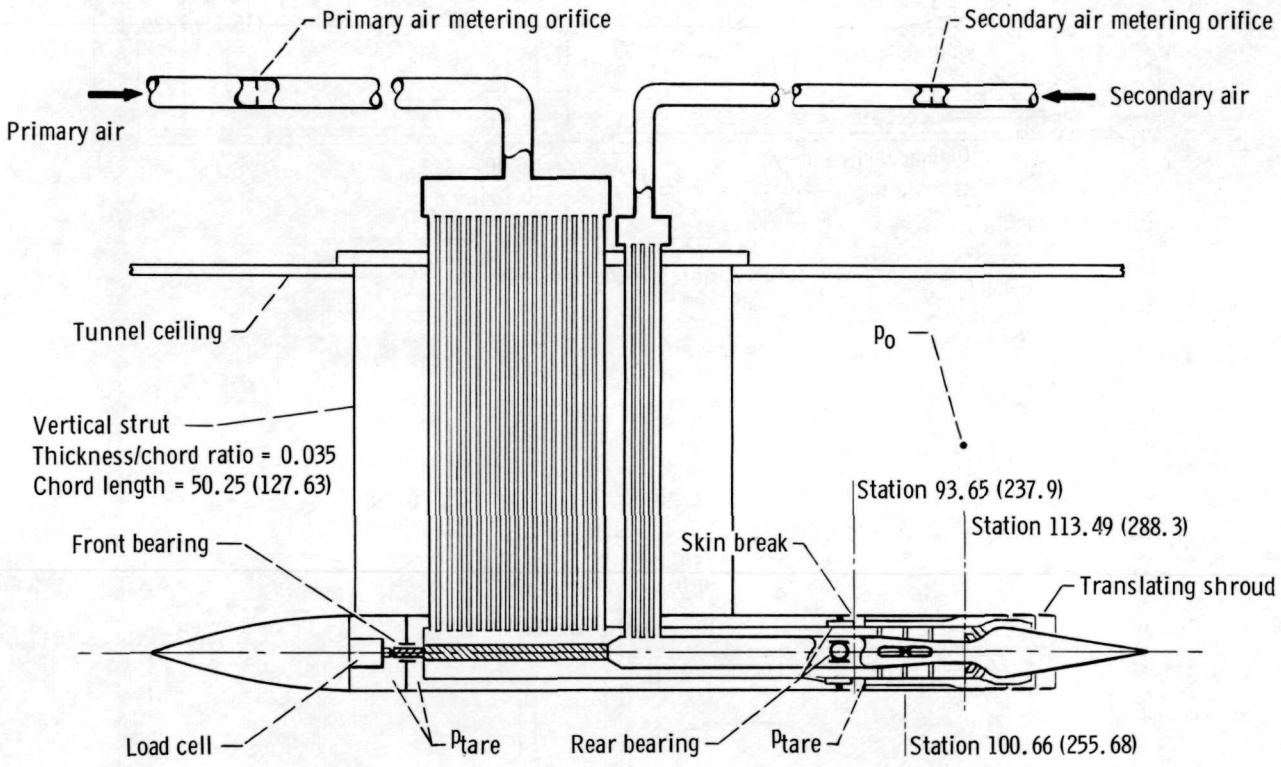

Figure 3. - Schematic view of nozzle support model and air supply systems for 8- by 6-Foot Supersonic Wind Tunnel. (Dimensions are in inches (cm).)

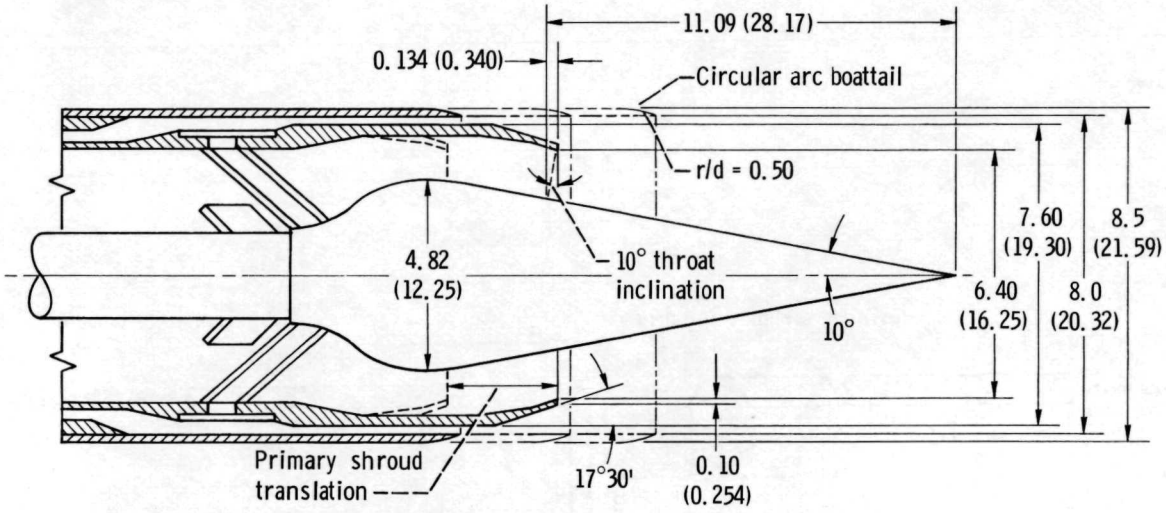

(a) Plug nozzle model dimensions.

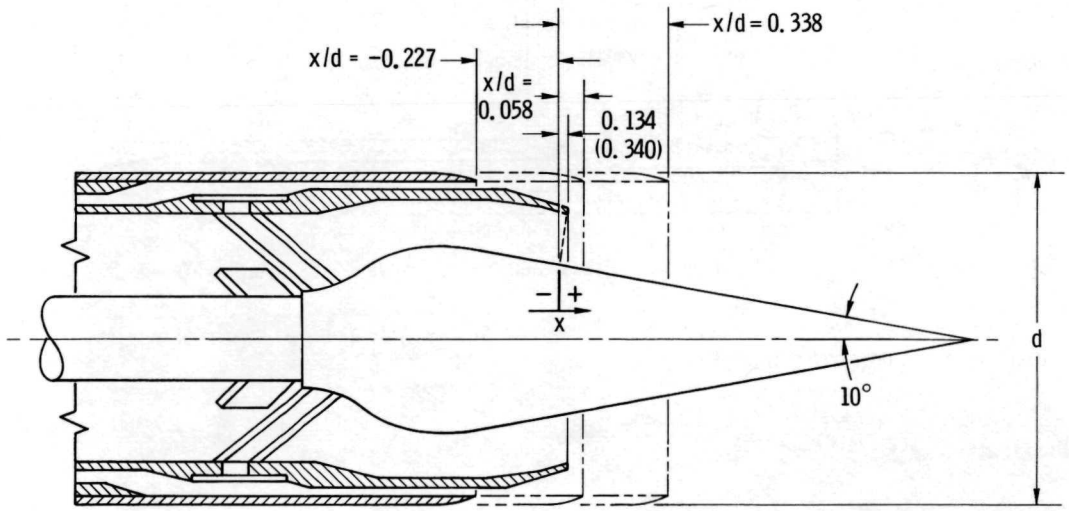

(b) Plug nozzle secondary shroud locations.

CD-10172-28

Figure 4. - Model dimensions and geometric variables. (Dimensions are in inches (cm) unless otherwise noted.)

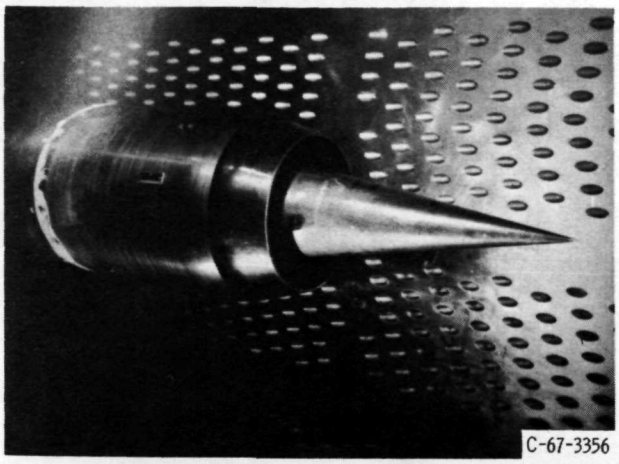

(a) Shroud length to diameter ratio, x/d = -0.227; internal area ratio, A_9/A_8 =1.0.

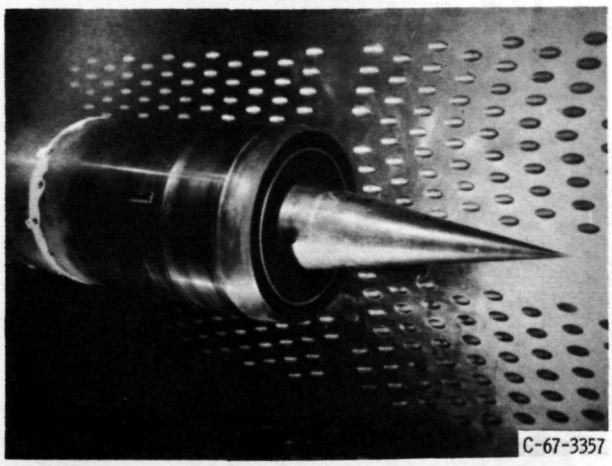

(b) Shroud length to diameter ratio, x/d = 0.058; internal area ratio, A_9/A_8 = 1.92.

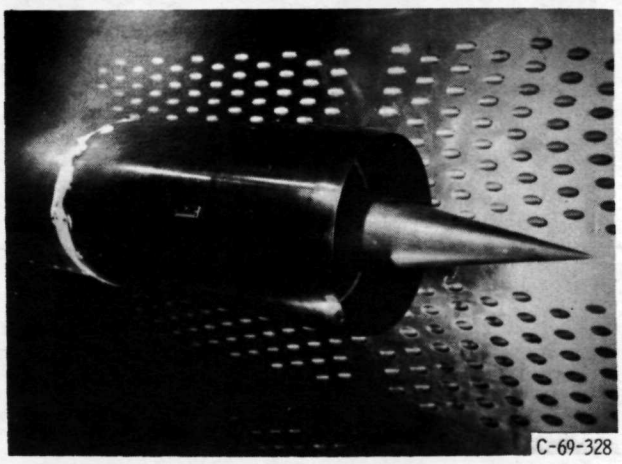

(c) Shroud length to diameter ratio, x/d = 0.338; internal area ratio, A_9/A_8 = 2.13.

Figure 5. - Full-length plug with translating secondary shroud.

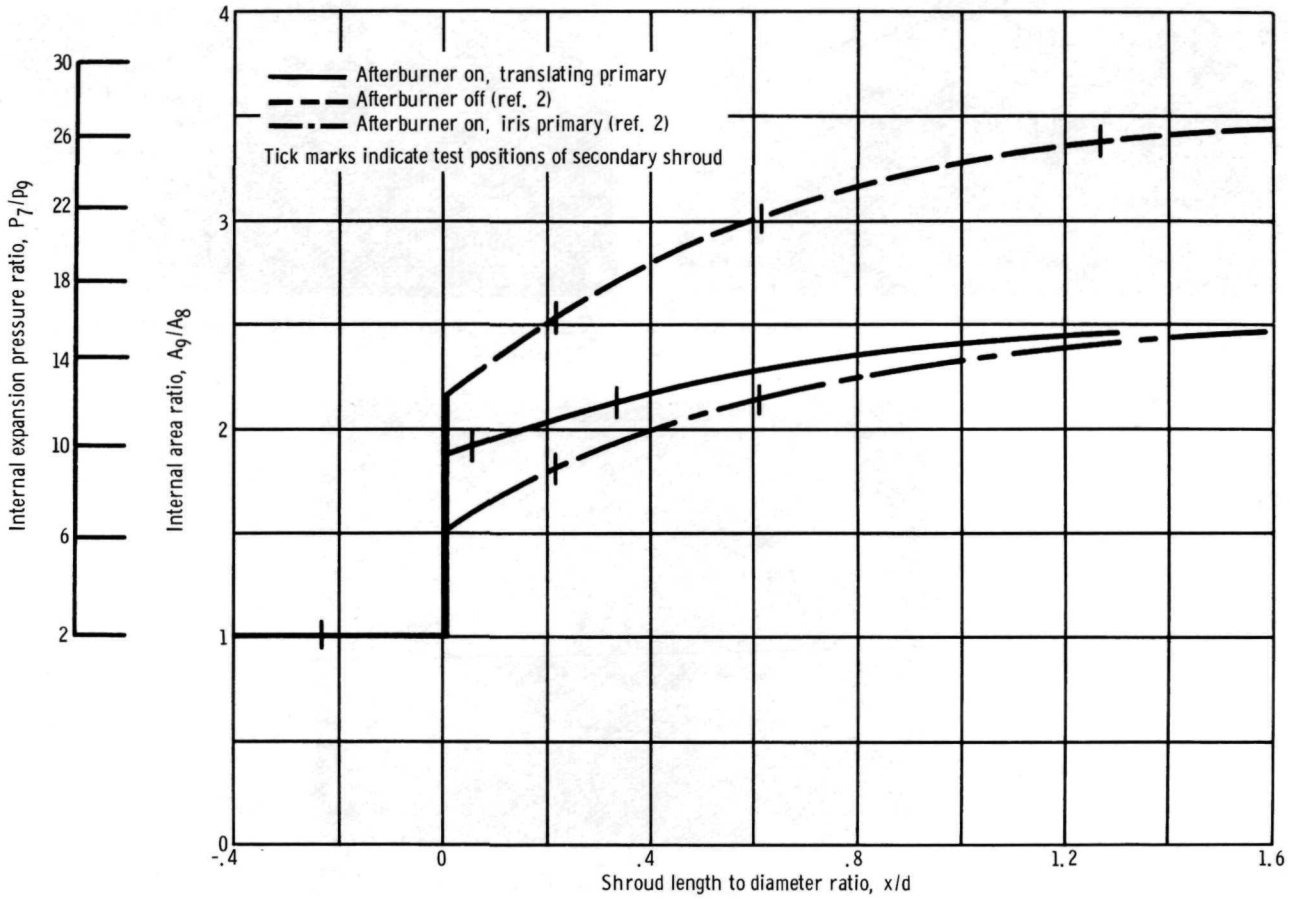

Figure 6. - Effect of secondary shroud translation on internal area ratio and pressure ratio.

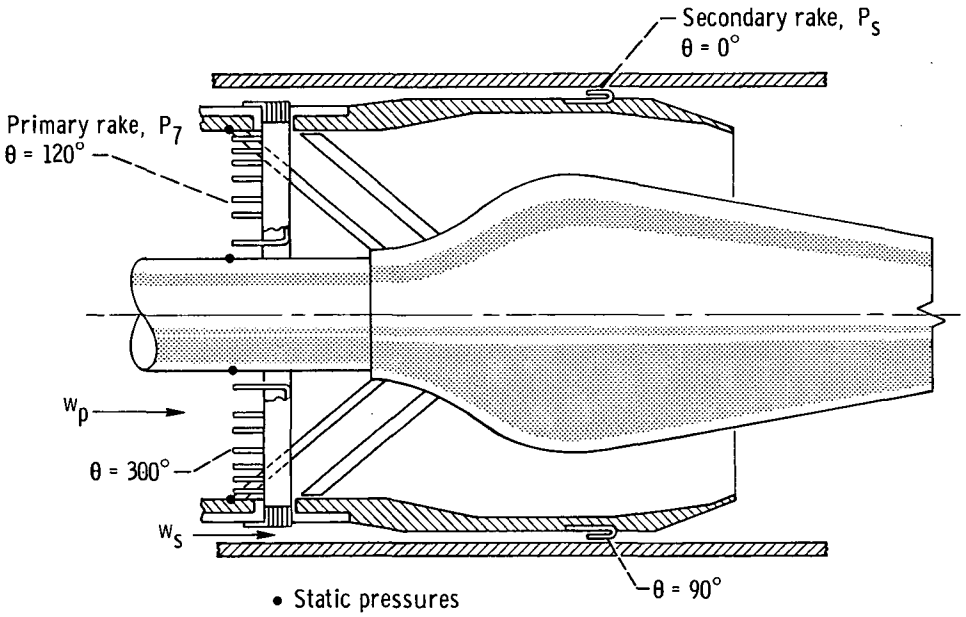

(a) Primary and secondary total-pressure rakes.

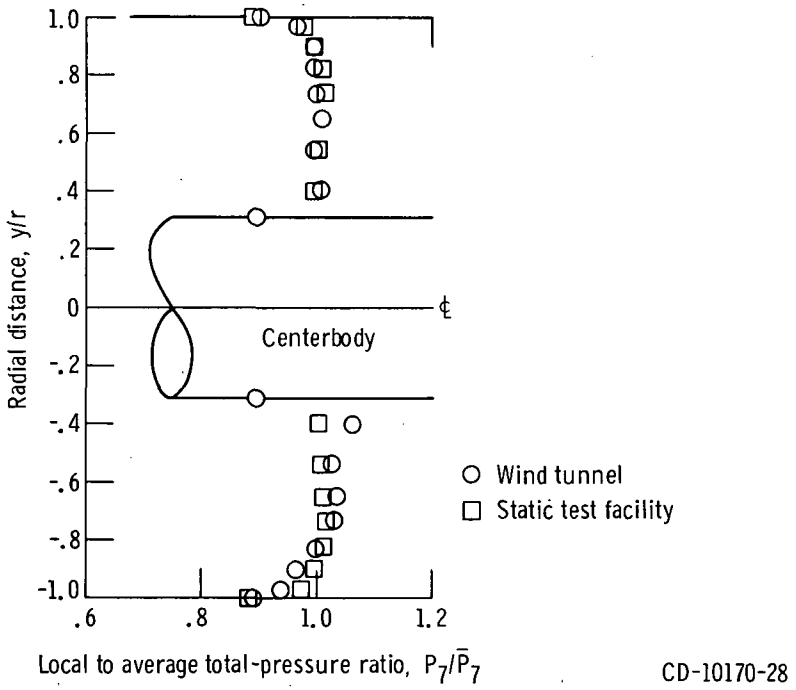

(b) Typical primary rake pressure profiles.

Figure 7. - Model instrumentation.

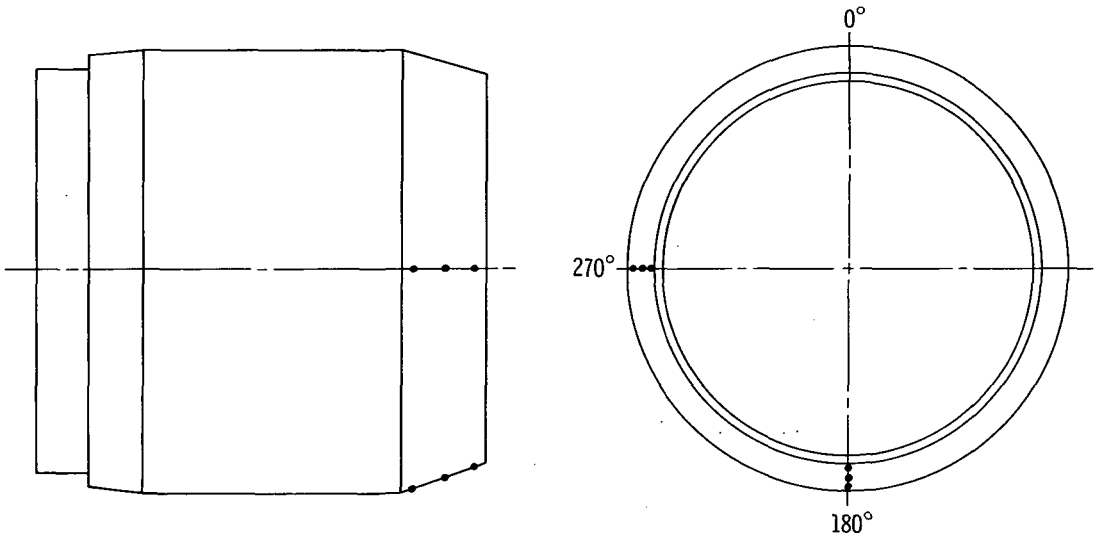

(c) Primary shroud boattail static pressures.

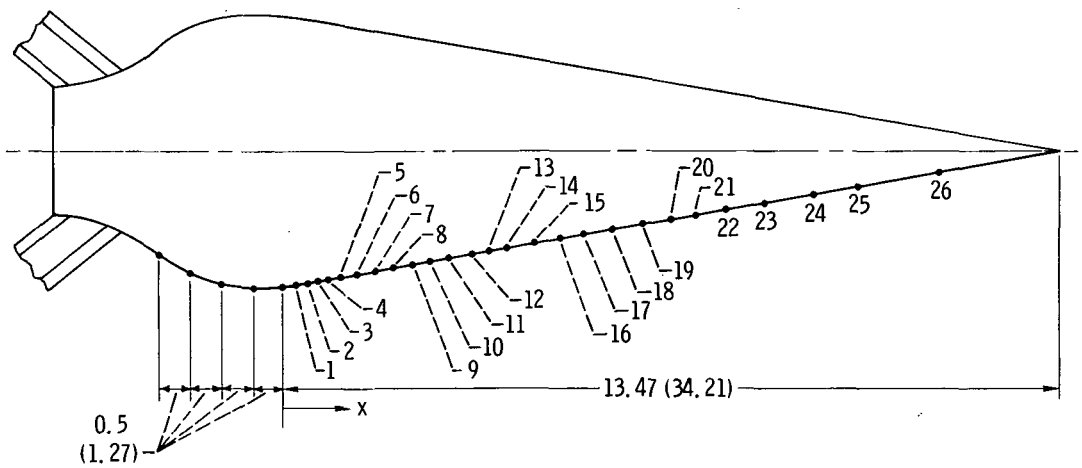

Orifice	Axial distance from nozzle throat with afterburner off, x		Orifice	Axial distance from nozzle throat with afterburner off, x		Orifice	Axial distance from nozzle throat with afterburner off, x	
	in.	cm		in.	cm		in.	cm
1	0.145	0.368	10	2.750	6.985	19	6.230	15.824
2	.405	1.029	11	3.080	7.823	20	6.735	17.107
3	.675	1.714	12	3.400	8.636	21	7.270	18.466
4	.955	2.426	13	3.750	9.525	22	7.850	19.939
5	1.235	3.137	14	4.115	10.452	23	8.505	21.603
6	1.525	3.873	15	4.500	11.430	24	9.270	23.546
7	1.840	4.674	16	4.890	12.421	25	10.210	25.933
8	2.140	5.436	17	5.315	13.500	26	11.590	29.439
9	2.430	6.172	18	5.770	14.656			

(d) Plug static-pressure locations. (All dimensions are in inches (cm) unless otherwise noted.)

Figure 7. - Concluded.

CD-10171-28

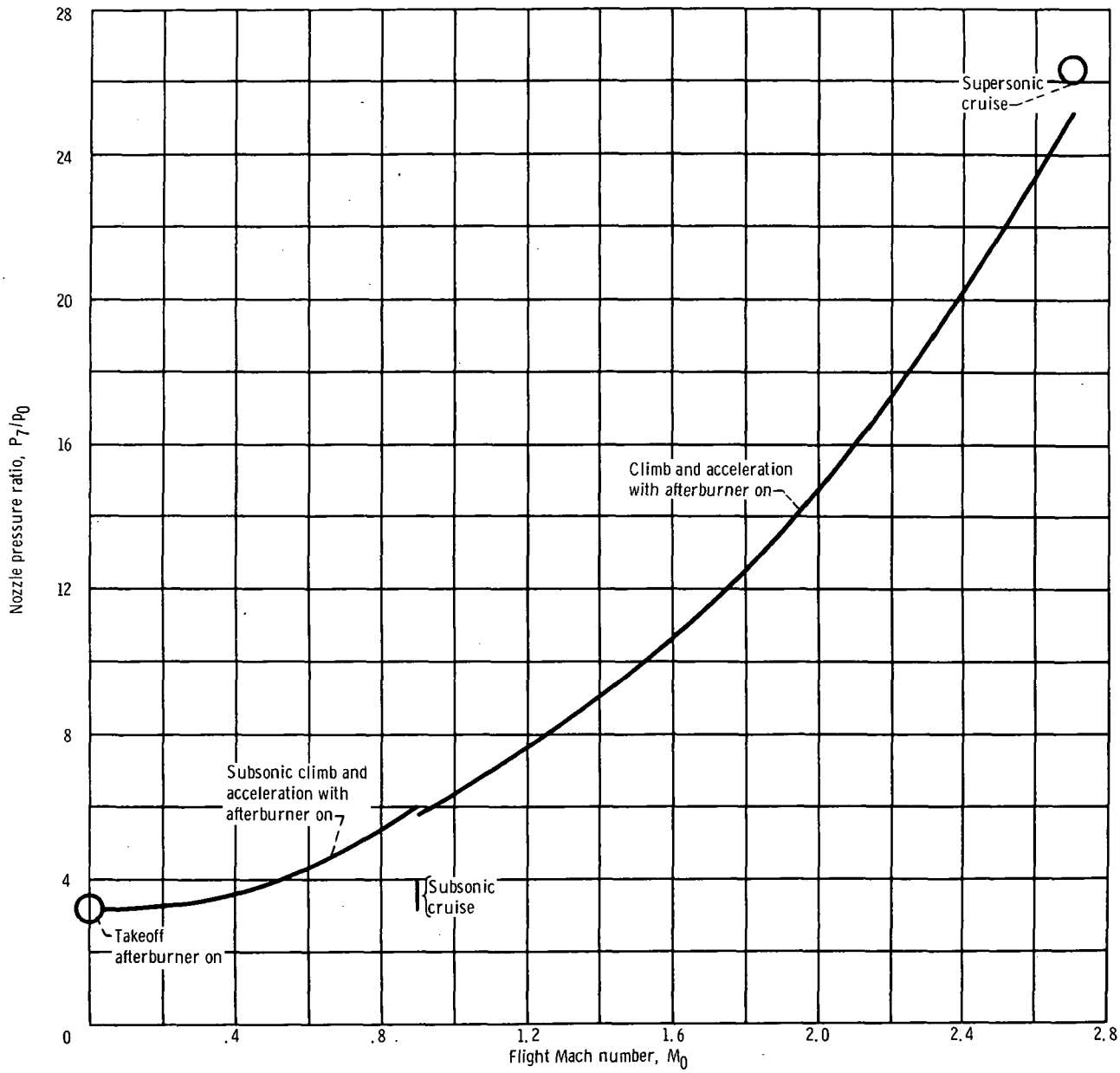

Figure 8. - Pressure ratio schedule for typical turbojet engine.

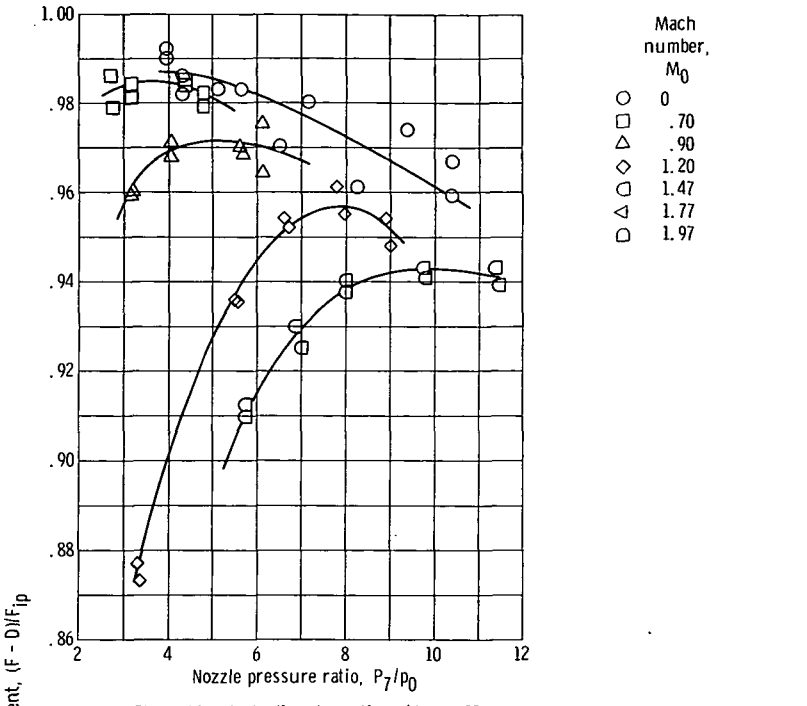

(a) Shroud length to diameter ratio, x/d = -0.227; internal area ratio, $A_9/A_8 = 1.0$.

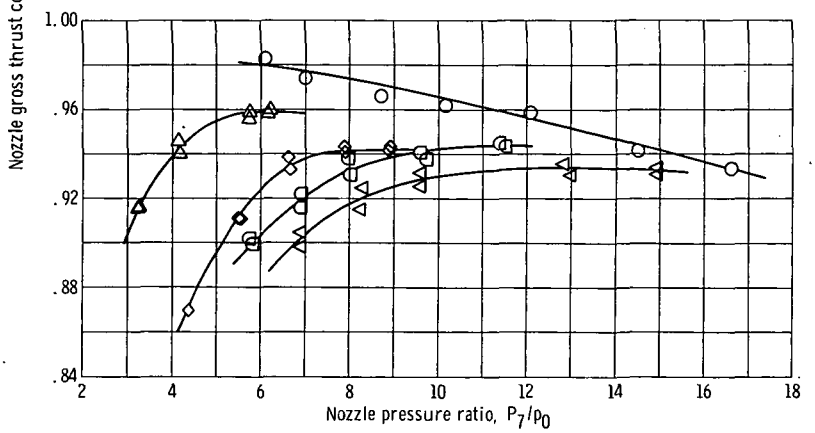

(b) Shroud length to diameter ratio, x/d = 0.058; internal area ratio, $A_9/A_8 = 1.92$.

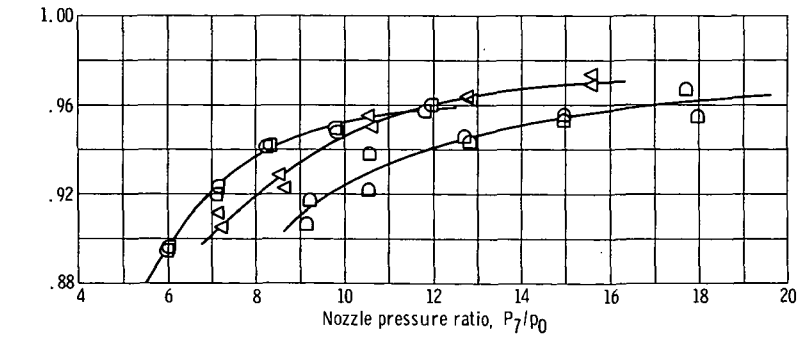

(c) Shroud length to diameter ratio, x/d = 0.338; internal area ratio, $A_9/A_8 = 2.13$.

Figure 9. - External flow effect on full-length plug nozzle performance; afterburner on; corrected secondary flow ratio, $(w_s/w_p)\sqrt{T_s/T_p} = 0$.

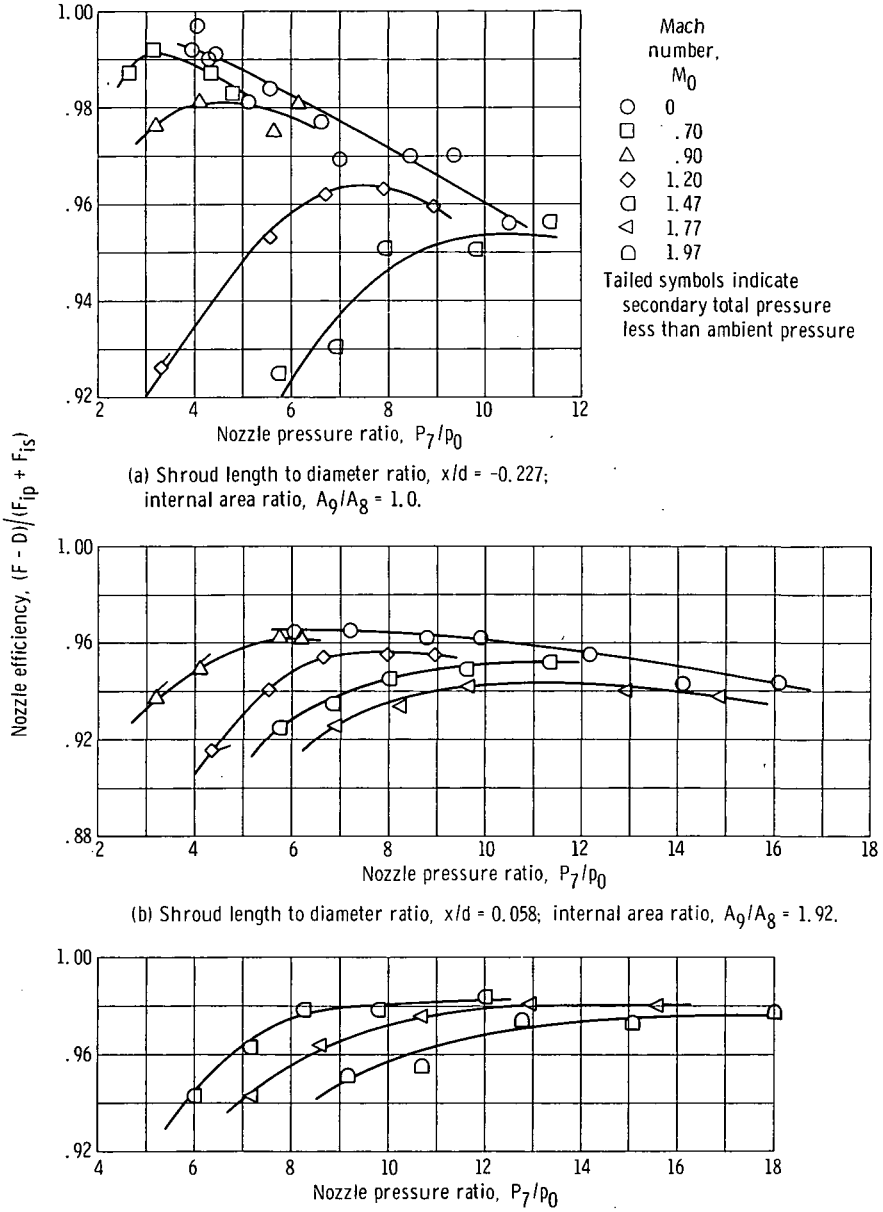

(a) Shroud length to diameter ratio, x/d = -0.227; internal area ratio, A_9/A_8 = 1.0.

(b) Shroud length to diameter ratio, x/d = 0.058; internal area ratio, A_9/A_8 = 1.92.

(c) Shroud length to diameter ratio, x/d = 0.338; internal area ratio, A_9/A_8 = 2.13.

Figure 10. - External flow effect on full-length plug nozzle performance; afterburner on, corrected secondary flow ratio, $(w_s/w_p)\sqrt{T_s/T_p}$ = 4 percent.

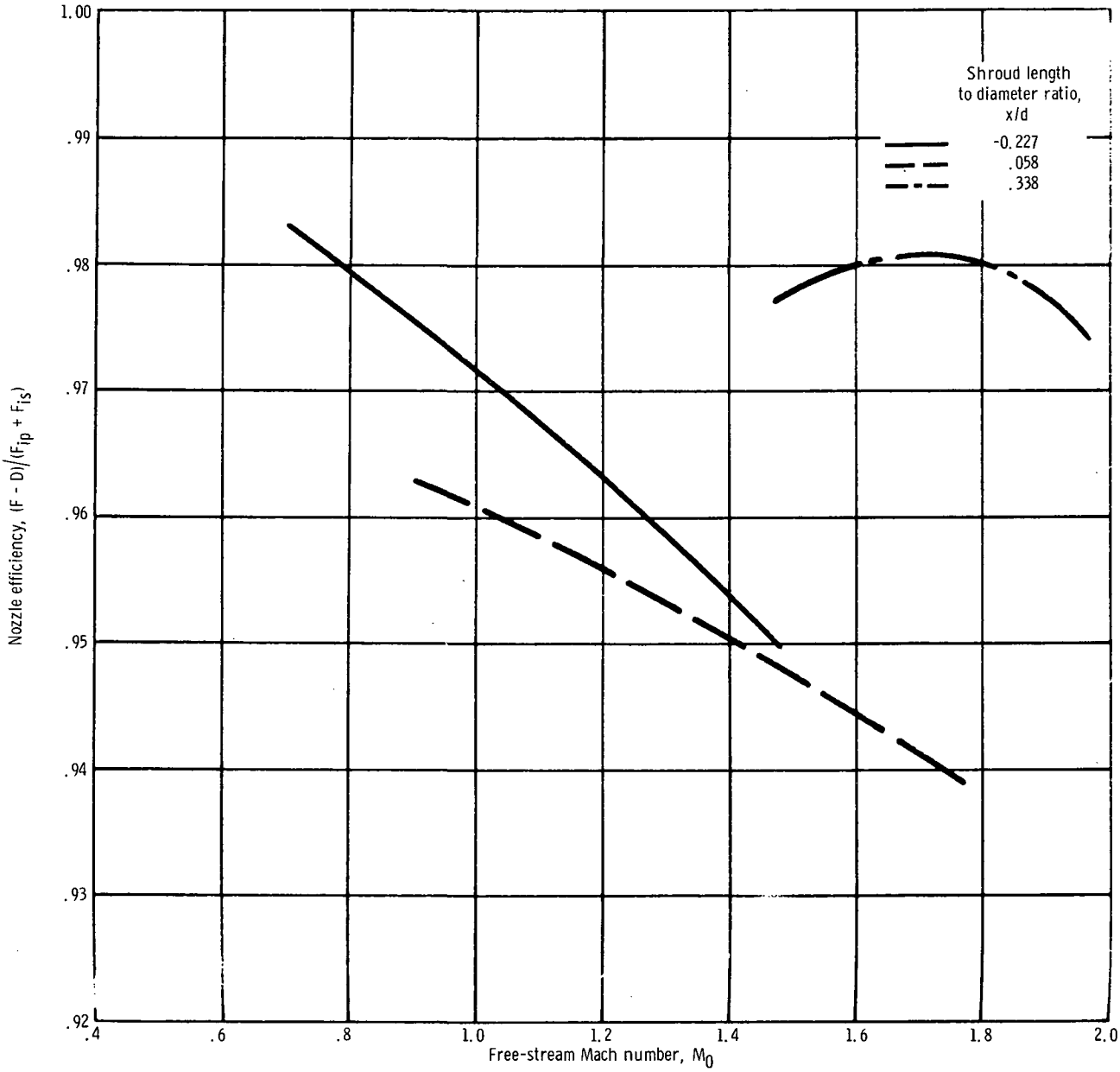

Figure 11. - Comparison of nozzle efficiency for three secondary shroud positions. Corrected secondary weight flow ratio, $(w_s/w_p)\sqrt{T_s/T_p}$ = 4 percent.

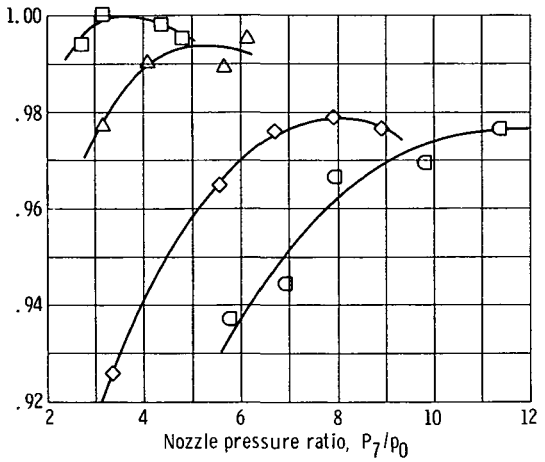

(a) Shroud length to diameter ratio, x/d = -0.227; internal area ratio, A_9/A_8 = 1.0.

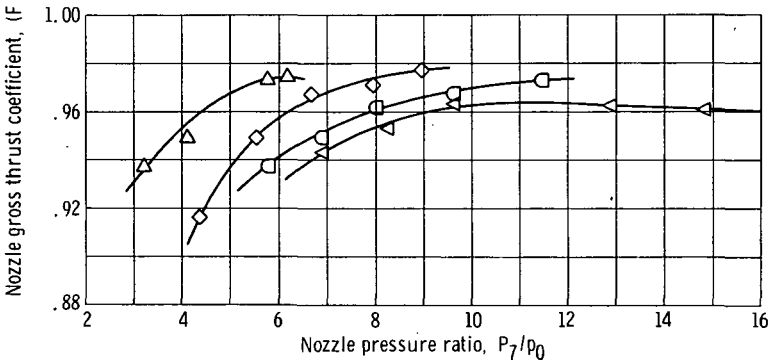

(b) Shroud length to diameter ratio, x/d = 0.058; internal area ratio, A_9/A_8 = 1.92.

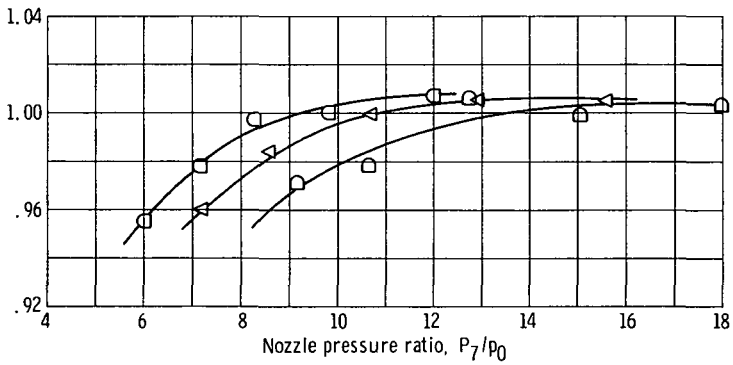

(c) Shroud length to diameter ratio, x/d = 0.338; internal area ratio, A_9/A_8 = 2.13.

Figure 12. - External flow effect on full-length plug nozzle gross thrust coefficient. Afterburner on; corrected secondary flow ratio, $(w_s/w_p)\sqrt{T_s/T_p}$ = 4 percent.

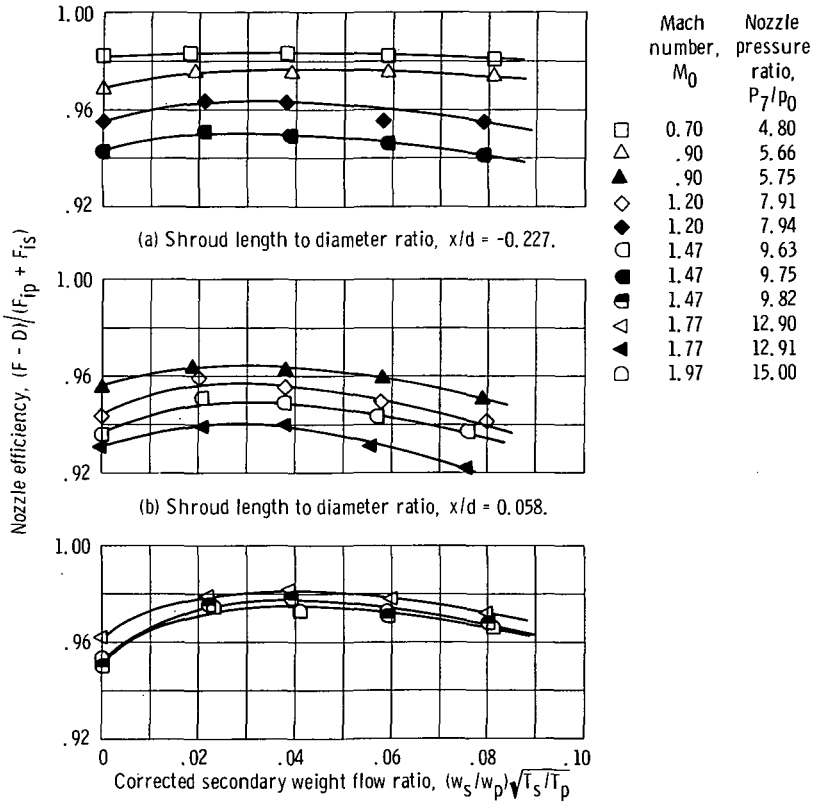

Figure 13. - Effect of secondary flow on performance of full-length plug nozzle with translated primary shroud.

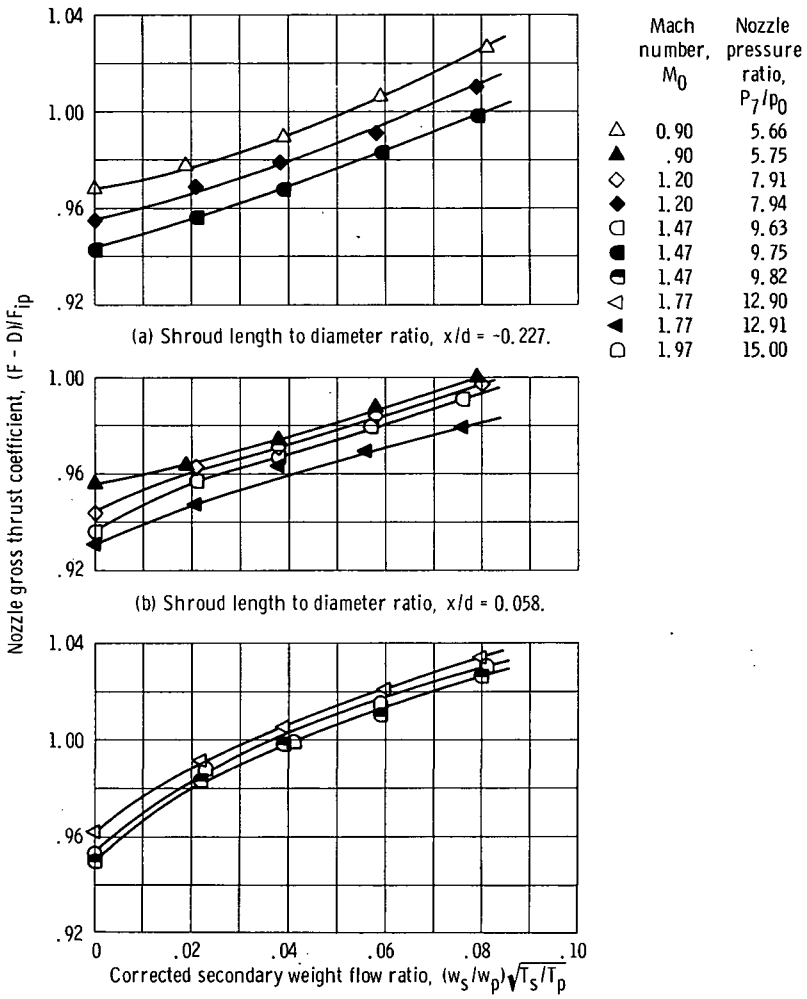

Figure 14. - Effect of secondary flow on nozzle gross thrust coefficient of full-length plug nozzle with translated primary shroud.

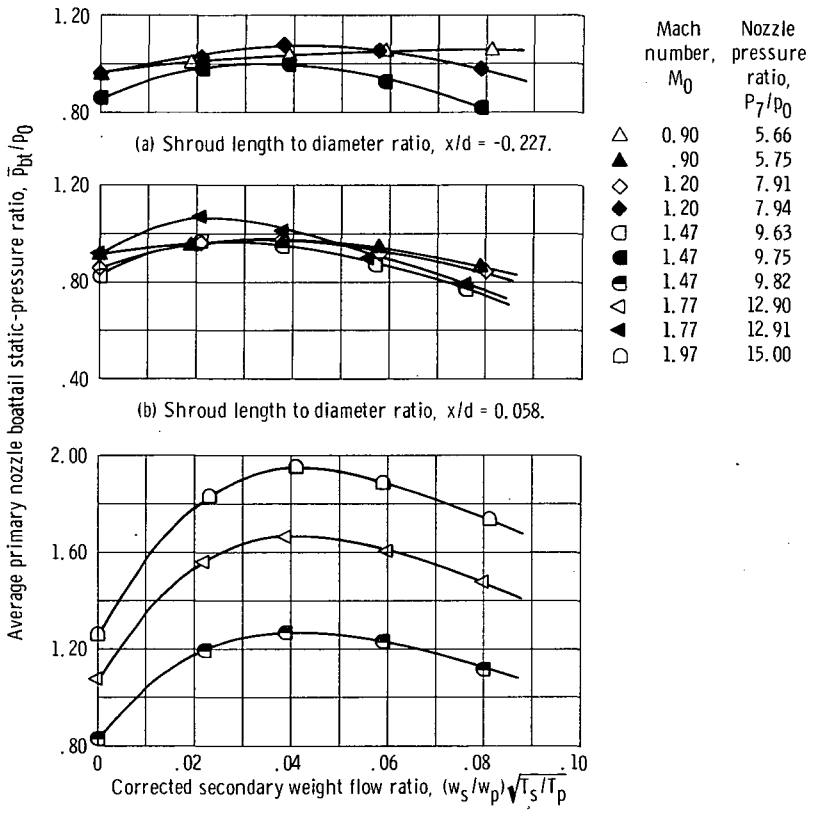

Figure 15. - Effect of secondary flow on primary shroud boattail pressures of full-length plug nozzle with translated primary shroud.

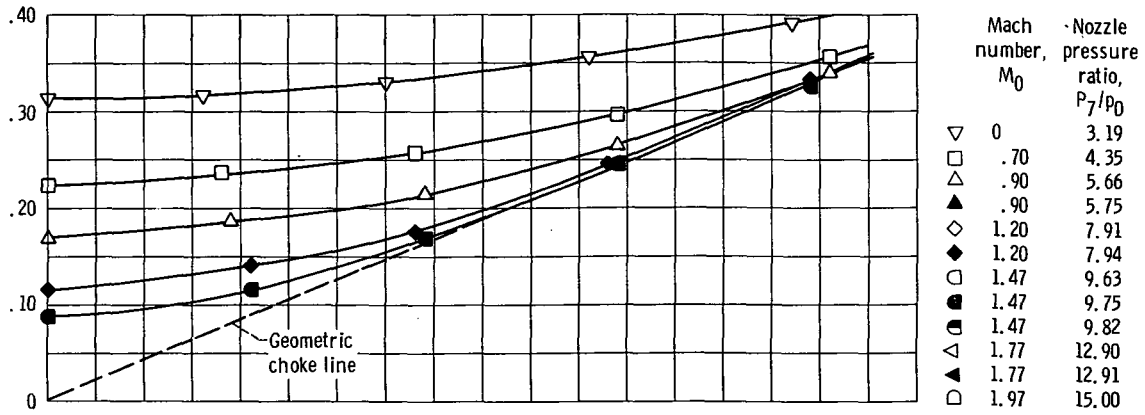

(a) Shroud length to diameter ratio, x/d = -0.227.

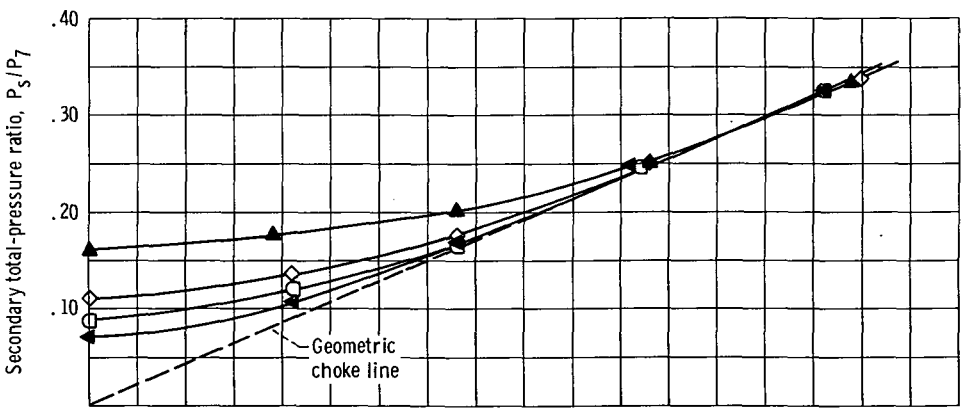

(b) Shroud length to diameter ratio, x/d = 0.058.

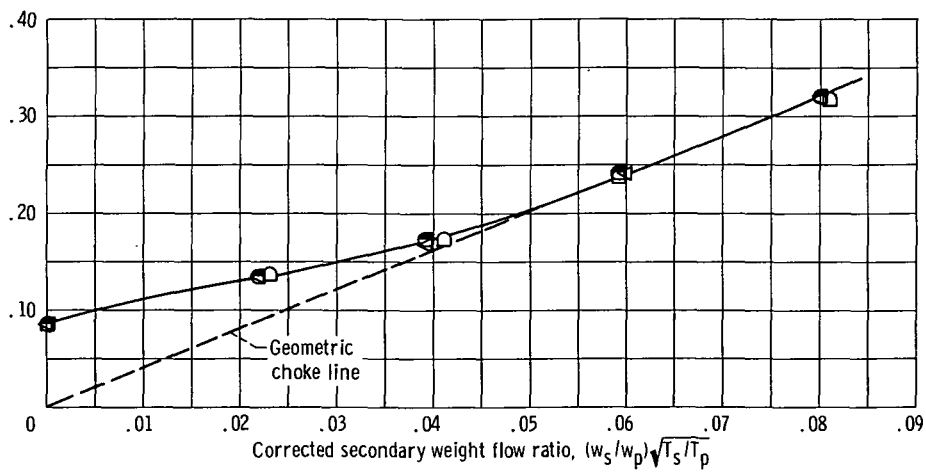

(c) Shroud length to diameter ratio, x/d = 0.338.

Figure 16. - Pumping characteristic curves for translated primary shroud.

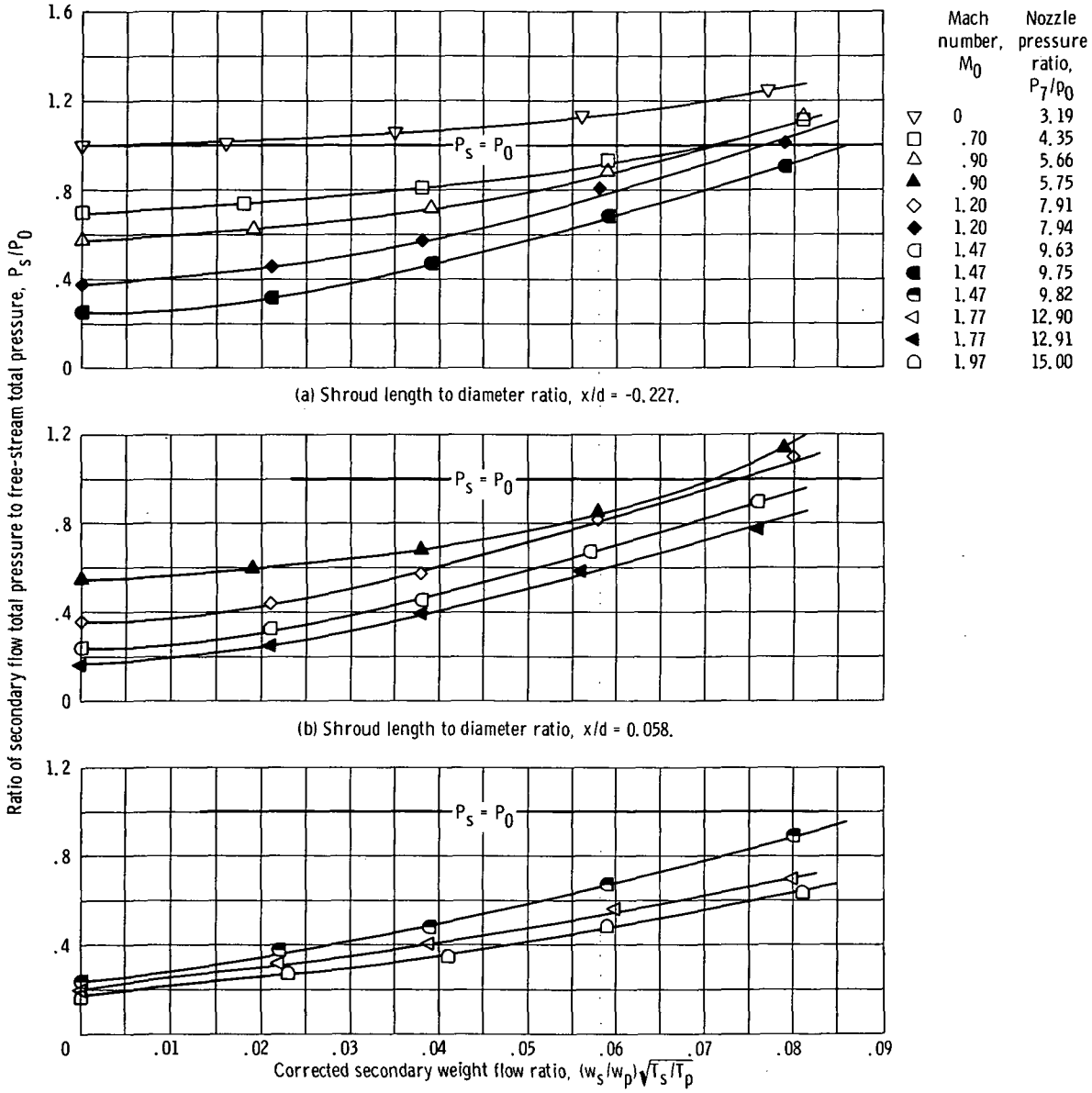

(a) Shroud length to diameter ratio, x/d = -0.227.

(b) Shroud length to diameter ratio, x/d = 0.058.

(c) Shroud length to diameter ratio, x/d = 0.338.

Figure 17. - Secondary flow pressure recovery requirement for full-length plug nozzle with translated primary shroud.

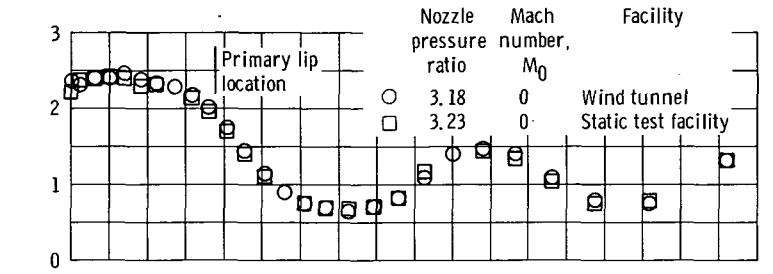

(a) Shroud length to diameter ratio, x/d = -0.227. Nominal pressure ratio, 3.2.

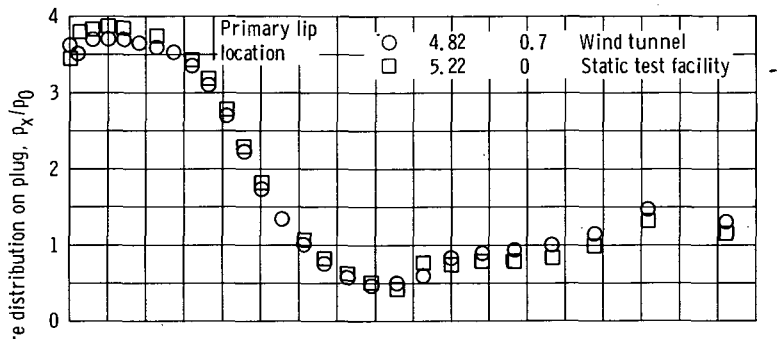

(b) Shroud length to diameter ratio, x/d = -0.227. Nominal pressure ratio, 5.0.

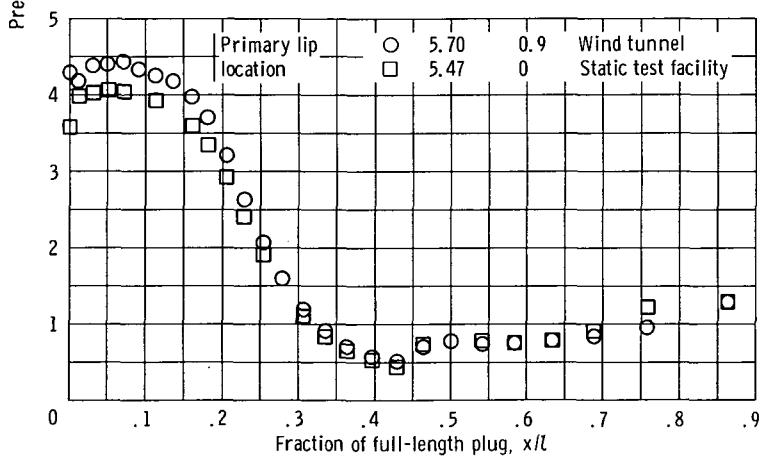

(c) Shroud length to diameter ratio, x/d = -0.227. Nominal pressure ratio, 5.6.

Figure 18. - Effect of external flow on plug pressure distribution. Translated primary shroud, corrected secondary flow ratio, $(w_s/w_p)\sqrt{T_s/T_p} = 0$.

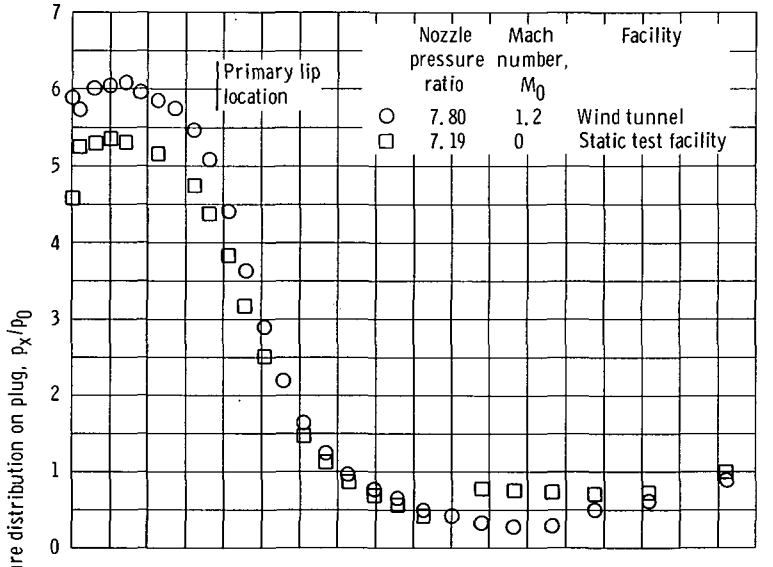

(d) Shroud length to diameter ratio, x/d = -0.227. Nominal pressure ratio, 7.5.

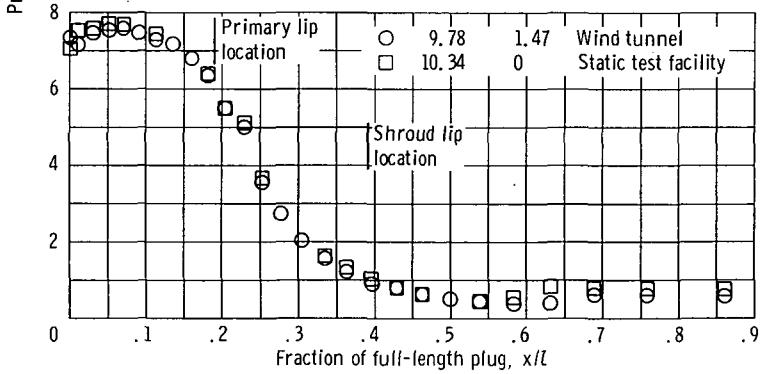

(e) Shroud length to diameter ratio, x/d = 0.338. Nominal pressure ratio, 10.0.

Figure 18. - Continued.

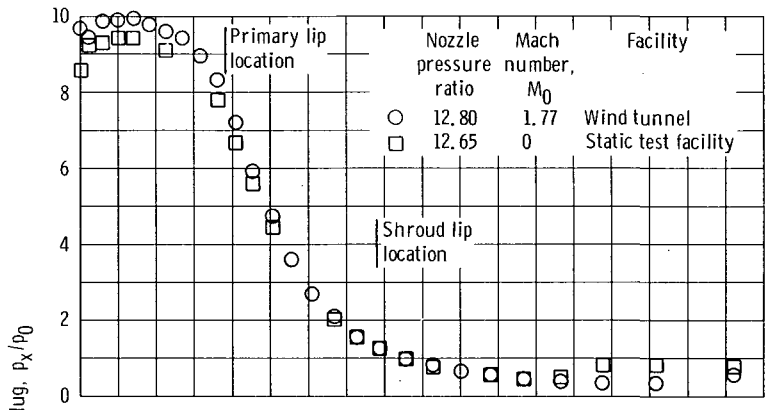

(f) Shroud length to diameter ratio, x/d = 0.338. Nominal pressure ratio, 12.75.

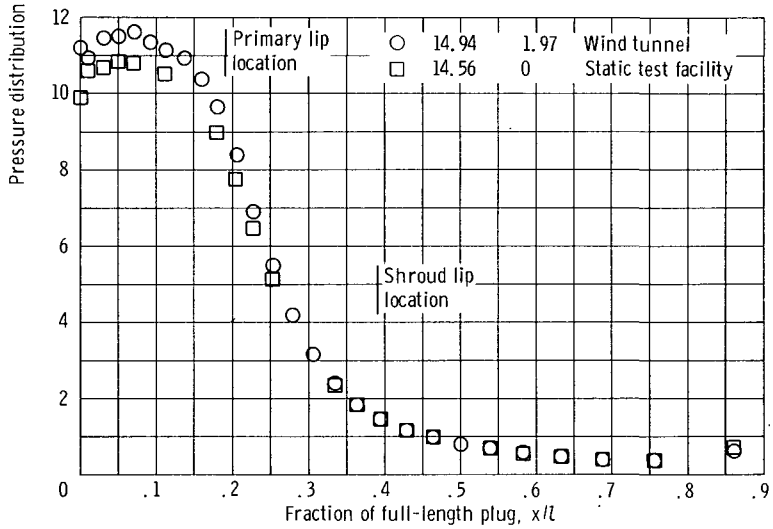

(g) Shroud length to diameter ratio, x/d = 0.338. Nominal pressure ratio, 14.75.

Figure 18. - Concluded.

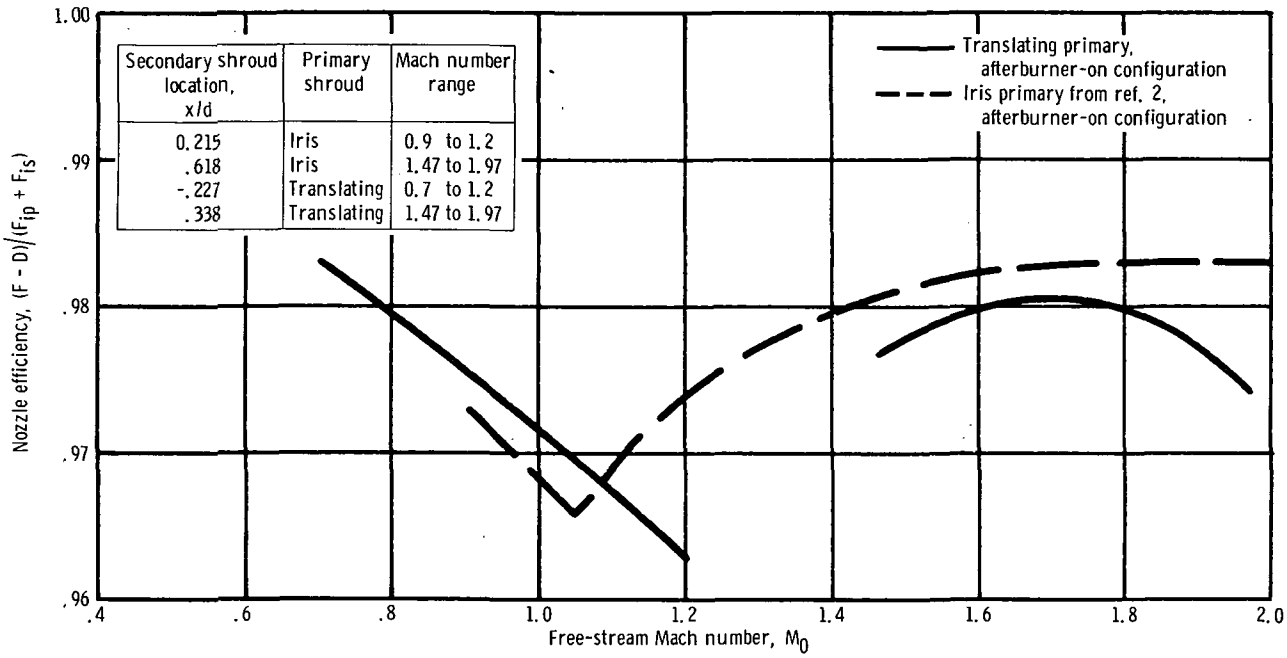

Figure 19. - Comparison of nozzle performance for two methods of throat area variation over flight Mach number range. Corrected secondary flow ratio, $(w_s/w_p)\sqrt{T_s/T_p} = 4$ percent.

NASA-Langley, 1969 —— 28 E-4749

"The aeronautical and space activities of the United States shall be conducted so as to contribute . . . to the expansion of human knowledge of phenomena in the atmosphere and space. The Administration shall provide for the widest practicable and appropriate dissemination of information concerning its activities and the results thereof."

—NATIONAL AERONAUTICS AND SPACE ACT OF 1958

NASA SCIENTIFIC AND TECHNICAL PUBLICATIONS

TECHNICAL REPORTS: Scientific and technical information considered important, complete, and a lasting contribution to existing knowledge.

TECHNICAL NOTES: Information less broad in scope but nevertheless of importance as a contribution to existing knowledge.

TECHNICAL MEMORANDUMS: Information receiving limited distribution because of preliminary data, security classification, or other reasons.

CONTRACTOR REPORTS: Scientific and technical information generated under a NASA contract or grant and considered an important contribution to existing knowledge.

TECHNICAL TRANSLATIONS: Information published in a foreign language considered to merit NASA distribution in English.

SPECIAL PUBLICATIONS: Information derived from or of value to NASA activities. Publications include conference proceedings, monographs, data compilations, handbooks, sourcebooks, and special bibliographies.

TECHNOLOGY UTILIZATION PUBLICATIONS: Information on technology used by NASA that may be of particular interest in commercial and other non-aerospace applications. Publications include Tech Briefs, Technology Utilization Reports and Notes, and Technology Surveys.

Details on the availability of these publications may be obtained from:

SCIENTIFIC AND TECHNICAL INFORMATION DIVISION
NATIONAL AERONAUTICS AND SPACE ADMINISTRATION
Washington, D.C. 20546